Article:

Gibson, M.J., Glasser, N.F., Quincey, D.J. et al. (3 more authors) (2017) Temporal variations in supraglacial debris distribution on Baltoro Glacier, Karakoram between 2001 and 2012. Geomorphology, 295. pp. 572-585. ISSN 0169-555X

https://doi.org/10.1016/j.geomorph.2017.08.012

Temporal variations in supraglacial debris distribution on Baltoro Glacier, Karakoram between 2001 and 2012

Morgan J. Gibson[1*], Neil F. Glasser[1], Duncan J. Quincey[2], Christoph Mayer[3], Ann V. Rowan[4], Tristram D.L. Irvine-Fynn[1],

[1]Department of Geography and Earth Sciences, Aberystwyth University, Aberystwyth, UK
[2]School of Geography, University of Leeds, Leeds, UK
[3]Commision for Geodesy and Glaciology, Bavarian Academy of Sciences and Humanities, Munich, Germany.
[4]Department of Geography, University of Sheffield, Sheffield, UK

*Corresponding author: mog2@aber.ac.uk

Abstract

Distribution of supraglacial debris in a glacier system varies spatially and temporally due to differing rates of debris input, transport and deposition. Supraglacial debris distribution governs the thickness of a supraglacial debris layer, an important control on the amount of ablation that occurs under such a debris layer. Characterising supraglacial debris layer thickness on a glacier is therefore key to calculating ablation across a glacier surface. The spatial pattern of debris thickness on Baltoro Glacier has previously been calculated for one discrete point in time (2004) using satellite thermal data and an empirically based relationship between supraglacial debris layer thickness and debris surface temperature identified in the field. Here, the same empirically based relationship was applied to two further datasets (2001, 2012) to calculate debris layer thickness across Baltoro Glacier for three discrete points over an 11-year period (2001, 2004, 2012). Surface velocity and sediment flux were also calculated, as well as debris thickness change between periods. Using these outputs, alongside geomorphological maps of Baltoro Glacier produced for 2001, 2004 and 2012, spatiotemporal changes in debris distribution for a sub-decadal timescale were investigated. Sediment flux remained constant throughout the 11-year period. The greatest changes in debris thickness occurred along medial moraines, the locations of mass movement deposition and areas of interaction between tributary glaciers and the main glacier tongue. The study confirms the occurrence of spatiotemporal changes in supraglacial debris layer thickness on sub-decadal timescales, independent of variation in surface velocity. Instead, variation in rates of debris distribution are primarily attributed to frequency and magnitude of mass movement events over decadal timescales, with climate, regional uplift and erosion rates expected to control debris inputs over centurial to millennial timescales. Inclusion of such spatiotemporal variations in debris thickness in distributed surface energy balance models would increase the accuracy of calculated ablation, leading

to a more accurate simulation of glacier mass balance through time, and greater precision in quantification of the response of debris-covered glaciers to climatic change.

Keywords: Karakoram, debris-covered glaciers, supraglacial debris, Baltoro Glacier

1. Introduction

Debris-covered glaciers are commonly found in tectonically-active mountain ranges including the Andes, the Southern Alps of New Zealand and the Himalaya-Karakoram (Kirkbride, 1999; Scherler et al., 2011). High rates of rock uplift and erosion and steep hillslopes in these regions cause large volumes of rock debris to be incorporated into glacier systems, and ultimately form supraglacial debris layers of varying thicknesses and extents (Anderson and Anderson, 2016; Shroder et al., 2000). The presence of a supraglacial debris layer affects ablation of the underlying ice (Evatt et al., 2015; Östrem, 1959), because the debris acts as a thermal barrier between ice and atmosphere, ultimately resulting in a non-linear response of debris-covered glaciers to climatic change (Benn et al., 2012; Scherler et al., 2011). Glaciers in the Himalaya-Karakoram supply water to some of the largest rivers in the world, including the Indus, Brahmaputra and Ganges (Bolch et al., 2012). Consequently, the response of glaciers in the Himalaya-Karakoram to recent and current climatic change will affect the lives of the 1.4 billion people in central Asia who rely on these rivers as their primary water resource (Immerzeel et al., 2010).

Given that the proportion of debris-covered glacier ice area in the Himalaya-Karakoram region is increasing (Deline, 2005; Mihalcea et al., 2006), gaining a full understanding of the influence of debris layers on melt-rates is becoming increasingly pertinent. Typically, supraglacial debris is initially entrained into lateral and medial moraines in the upper reaches of the glacier. As moraines coalesce with increasing distance from their source the debris layer becomes more spatially extensive (Anderson, 2000; Kirkbride and Deline, 2013). The thickness of the supraglacial debris layer increases down-glacier and reaches its maximum near the glacier terminus (Anderson, 2000). In areas where supraglacial debris cover extends across the entire glacier surface spatially variable debris distribution results in differential melting and forms an undulating glacier surface topography (Hambrey et al., 2008; Kirkbride and Deline, 2013). Supraglacial debris thickness varies in space and time as a result of differing spatial extents and temporal rates of debris input, transport and exhumation (Rowan et al., 2015). Ablation rates of debris-covered glaciers are therefore also spatially and temporally variable (Benn et al., 2012; Rounce and McKinney, 2014). Studies that consider the response of debris-covered glaciers to climatic change currently do not account for this variability (e.g. Bolch et al., 2012; Scherler et al., 2011; Shea et al., 2015), which increases the uncertainty in estimations of glacier ablation rates, and thus the subsequent predictions of the response of debris-covered glaciers to climatic change.

The impact of supraglacial debris layers on melt rates is well established (e.g. Östrem, 1959); thin debris layers (typically <0.05 m thick, depending on local conditions) enhance ablation by increasing albedo of the glacier surface, while thicker debris layer attenuate melt by insulation of the underlying ice (Mihalcea et al., 2008b; Nicholson and Benn, 2006; Östrem, 1959). Ablation is maximized at an effective debris thickness (commonly 0.01–0.02 m), while the critical thickness of debris (ranging from 0.02 to 0.1 m), where ablation under debris-covered ice is equal to that of debris-free ice, is defined by debris properties such as lithology, porosity, grain size distribution, moisture content and surface roughness of the debris layer (Brock et al., 2010; Kayastha et al., 2000). The amount of ablation under a debris layer is also affected by external factors such as the transfer rate of precipitation through a debris layer, glacier surface topography, and the occurrence of suprafluvial networks and associated sediment transport processes, all of which are spatially and temporally variable (Seong et al., 2009).

Measuring the thickness distribution of a supraglacial debris layer is challenging in the field due to high spatial variability in debris layer thickness over short distances, difficulties in excavating such debris layers (Mayer et al., 2006), and an inability to capture such variability with point data. Early work put forward the idea of using thermal characteristics of supraglacial debris to define its extent from satellite data (Ranzi et al., 2004). Subsequent projects developed the use of such thermal satellite data to estimate debris thickness for entire glacier surfaces: a glacier-specific relationship between surface temperature and debris thickness is identified using field point data, which is subsequently applied to satellite-derived thermal data of the entire glacier area (e.g. Foster et al., 2012; Rounce and McKinney, 2014; Mihalcea et al., 2008a; Mihalcea et al., 2008b; Soncini et al., 2016). These maps have advanced understanding of spatial variability in debris thickness, but usually only represent a discrete point in time. Minora et al. (2015) enabled the observation of temporal changes in debris thickness by producing a second debris thickness map of Baltoro Glacier for 2011, in addition to the one produced by Mihalcea et al. (2008b) for 2004. However, Minora et al. (2015) did not explore the extent of debris thickness change between the two periods. Consequently, little is known about the rate at which changes in supraglacial debris layer thickness occur, an essential parameter for understanding the transport of debris by ice flow and the localised redistribution of the debris over a glacier surface, which can be used to validate precise numerical modelling of the dynamics of debris-covered glaciers through time (e.g. Anderson and Anderson, 2016; Rowan et al., 2015).

In this study, we investigated supraglacial debris on Baltoro Glacier in Pakistan to: (1) identify the spatio-temporal variation in supraglacial debris distribution on Baltoro Glacier between 2001 and 2012; (2) consider some of the processes that control these variations in debris distribution using surface velocity and geomorphological mapping; and (3) calculate annual rates of debris thickness change and sediment flux on Baltoro Glacier using debris thickness and surface velocity maps. We subsequently comment on how such calculations can be used in numerical models for glaciers.

2. Study area

Baltoro Glacier is located in the eastern Karakoram mountain range in northern Pakistan (35°35' N, 76°04' E; Figure 1). The glacier is 62 km long and flows from near the peak of K2 (8611 m a.s.l.) to an altitude of 3410 m a.s.l. (Mayer et al., 2006; Mihalcea et al., 2008b) (Figure 1a). A number of tributary glaciers feed Baltoro Glacier (Figure 1b), including Baltoro South and Godwin-Austen Glaciers, which converge to form the main Baltoro Glacier tongue at Concordia (4600 m). The surface velocity of Baltoro Glacier varies along its length, with a maximum surface velocity of ~200 m a^{-1} below Concordia, decreasing to less than 15 m a^{-1} close to the glacier terminus (Copland et al., 2009; Quincey et al., 2009). Surface velocity was observed to increase in 2005 (Quincey et al., 2009), attributed to an abundance of meltwater being routed to the bed and thus reducing basal friction.

The ablation area of Baltoro Glacier is almost entirely debris covered. Up-glacier of Concordia, supraglacial debris is predominantly entrained into medial and lateral moraines that punctuate the clean ice surface, with a lesser contribution of mass movement deposits along the glacier margins (Mihalcea et al., 2006). The debris layer is thinnest (0.01–0.15 m) in the upper ablation area of the glacier and exceeds 1 m at the glacier terminus (Mihalcea et al., 2008b). Supraglacial debris units have differing lithologies across the debris-covered glacier surface, which include granite, schist, gneiss and metasediments (Gibson et al., 2016).

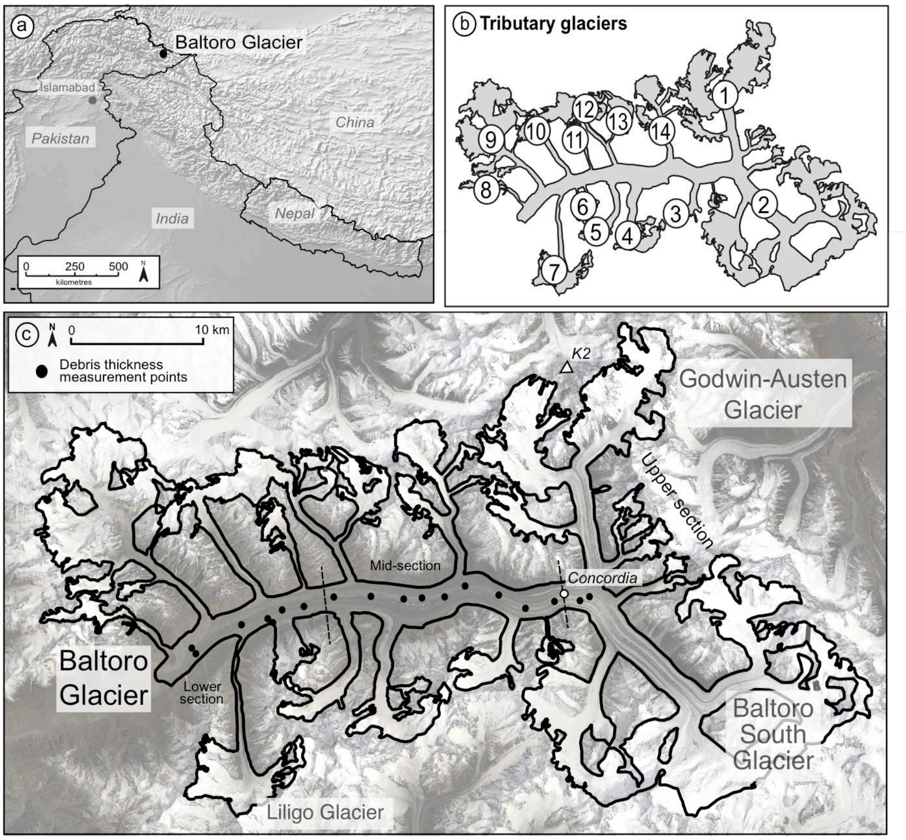

Figure 1. (a) Baltoro Glacier in a regional context; (b) the tributary glaciers of Baltoro Glacier (numbered) and (c) Baltoro Glacier and its tributary glaciers.

3. Methods

3.1. Debris thickness

Advanced Spaceborne Thermal Emission and Reflection Radiometer (ASTER) thermal data were used to derive debris thickness on Baltoro Glacier for three discrete periods in time; 2001, 2004 and 2012 (Table 1). The 2004 dataset was the same as that used by Mihalcea et al. (2008b) for production of their 2004 debris thickness map of Baltoro Glacier. The 2001 and 2012 data sets were chosen due to their low cloud cover, resulting in minimal glacier area being obscured. ASTER imagery was downloaded from NASA's Earth Observing System Data and Information System (http://reverb.echo.nasa.gov) as a Level 2 surface kinetic temperature product (AST_08). Level 2 surface kinetic temperature data are comprised of mean surface temperature calculated from thermal bands 11–15. Prior to delivery, surface kinetic temperature data are atmospherically corrected and converted from top-of-atmosphere temperature to surface temperature. ASTER thermal data have a spatial resolution of 90 m and temperature resolution of 0.5 K (Abrams and Ramachandran, 2002). The 2001 and 2012 ASTER datasets were both acquired in August within 15 days of the original 2004 dataset, therefore allowing for seasonal variation in debris surface to be minimised as much as possible when comparing subsequent outputs. All outputs were co-registered to within a pixel through manual placement of 50 tie points between each image pair prior to calculation of debris thickness, to avoid any spatial mismatch between the input layers. The images were also orthorectified using the rigourous orthorectification tool in ENVI (v. 5.0) and the ASTER digital elevation model (2011) at 30 m resolution, which corrects for the effect of sensor tilt and terrain, and produced an RMSE of 5.82 m. Debris thickness was derived using the methods detailed in Mihalcea et al. (2008b). Equation 1 was applied to the same satellite image used by Mihalcea et al. (2008b) to yield debris thickness for 2004:

$$\mathrm{DT} = \exp\left(0.0192\ \mathrm{T_S} - 58.7174\right) \quad (1)$$

Where DT is debris thickness and T_S is surface temperature. The same method was then applied to the 2001 and 2012 ASTER data for Baltoro Glacier to yield a time-series of debris thickness maps.

Table 1. Satellite ID, acquisition date and time and mean debris thickness for ASTER datasets used for calculating debris thickness (grey boxes) and surface velocity.

Satellite data I.D.	Acquisition date and time	Mean debris thickness (m)
AST_08_00308292001060003 _20140108123858_15605	29/08/2001 06:00	0.14
AST_08_00310032002055404 _20151109052624_814	03/09/2002 05:54	
AST_08_00308142004054614 _20151109052424_30691	14/08/2004 05:46	0.21
AST_08_00310122008054700 _20151109052644_888	12/09/2008 05:47	
AST_08_00305052011055248 _20151109052354_30515	05/09/2011 05:52	
AST_08_00308202012054630 _20151109052624_816	20/08/2012 05:46	0.45

Debris thickness change was calculated between the 2001–2004 and 2004–2012 debris thickness maps. In both cases the earlier debris thickness map was subtracted from the later map to yield debris thickness change for each time period, and then divided by the number of years between the two maps to calculate mean annual debris thickness change.

Uncertainty in the calculated debris thickness was estimated for the 2012 debris thickness map using field debris thickness measurements collected in 2013 (Figure 1c). Mean annual debris thickness change calculated from the 2004–2012 debris change map (0.03 m a^{-1}) was added to the 2012 debris thickness to provide projected debris thickness for 2013. To calculate uncertainty the 17 field-derived debris thickness point measurements were compared to debris thicknesses from the corresponding pixels in the projected 2013 debris thickness map (Table 2). Mean variation in debris thickness between 2013 field data and projected 2013 debris thickness was 0.090 m, 0.064 m above the uncertainty calculated for the 2004 debris thickness map by Mihalcea et al. (2008b) of 0.026 m. Consequently, in this study uncertainties for the debris thickness maps were estimated as 0.026 m for 2004 and 0.090 m for 2012. Uncertainty for the 2001 debris thickness map could not be calculated due to a lack of field data collected prior to 2004. Additional parameters such as moisture content in and thermal inertia of the debris layer may have also affected estimations of supraglcial debris layer thickness calculated using Mihalcea et al.'s (2008b) method, but the low uncertainty values calculated here suggest they have minimal effect on the outputs presented.

Due to a lack of field data in debris layers with a thickness greater than 0.5 m uncertainty values calculated here are only applicable for debris layers with a thickness ≤ 0.5 m. Above 0.5 m debris surface temperature is considered independent of debris layer thickness (Nicholson and Benn, 2006). Consequently, analysis of these debris thickness maps is focused on areas of the glacier where debris thickness is ≤0.5 m, and analysis of debris thickness maps are presented alongside geomorphological evidence for justification.

Table 2. Comparison of field point debris thickness data to corresponding pixel value (plus one year's annual rate of debris thickness change), used to calculate error between the 2012 satellite-derived debris thickness map and field data.

Point I.D.	2013 *in situ* debris thickness (m)	2013 satellite-derived debris thickness (m)	Difference (m)
1	0.02	0.01	0.01
2	0.00	0.07	0.07
3	0.09	0.23	0.14
4	0.13	0.15	0.02
5	0.01	0.04	0.03
6	0.06	0.03	0.03
7	0.04	0.02	0.02
8	0.05	0.14	0.09
9	0.075	0.02	0.05
10	0.04	0.23	0.19
11	0.12	0.39	0.27
12	0.07	0.18	0.11
13	0.17	0.06	0.11
14	0.04	0.14	0.10
15	0.26	0.28	0.02
16	0.1	0.01	0.09
17	0.43	1.16	0.73
		Mean difference:	0.09
		Standard deviation:	0.50

3.2. Glacier dynamics and surface morphology

3.2.1. Surface velocity analysis

Glacier surface velocity analysis was undertaken in ENVI (v.5.0) using the feature tracking plugin tool Cosi-Corr (Leprince et al., 2007). Cosi-Corr is a Fourier-based image correlation tool that offers sub-pixel accuracy for the measurement of horizontal offsets (Scherler et al., 2011). ASTER Band 3N data (Visible Near Infrared, Wavelength: 0.760–0.860 nm, resolution: 15 m) were used for feature tracking. Image pairs used were acquired in 2001 and 2002, 2003 and 2004, and 2011 and 2012 (Table 1), and were co-registered to sub-pixel level prior to calculation of surface displacement. All results were converted to annual displacements for comparison. A variable window size between 128 and 64 pixels and a step size of one pixel was used for all velocity outputs, and absolute surface velocity derived from north-south and east-west velocity fields. North-south and east-west velocity fields were used for identification of direction of maximum surface velocity in the calculation of sediment flux. Velocity outputs were masked using a velocity threshold of 200 m a^{-1} to exclude erroneous results in ENVI (v. 5.0), and clipped to the extent of a manually-improved Baltoro Glacier outline based on the Randolph Glacier Inventory outline (v. 5.0; Arendt et al., 2012), used in Gibson et al. (2016) in ArcMap (v.10.1). Pixels with erroneous surface velocity values (less than zero or above 200 m a^{-1}, or pixels with substantially different velocity values to the surrounding pixels) were masked from the final surface velocity maps.

3.2.2. Geomorphological mapping

Geomorphological features on the surface of Baltoro Glacier, including debris units, mass movement deposits, supraglacial water bodies and crevasses, were mapped using the optical bands (15 m resolution) of the same three time-separated and orthorectified ASTER data sets used for deriving debris thickness (August 2001, 2004 and 2012). ASTER images were orthorectified using the ASTER digital elevation model at 30 m resolution. Additionally, a Landsat 7 Enhanced Thematic Mapper (ETM+) image, acquired in August 2001 at 30 m resolution, was used to map regions of the glacier covered in cloud in the ASTER August 2001 imagery. All satellite datasets used were co-registered prior to mapping. Features were mapped using a false-colour composite (Bands 3N, 2, 1) and were manually digitised in ESRI ArcGIS (v. 10.1). Debris units were classified using their differing spectral reflectance profiles (Figure 2; Lillesand et al., 2014). The debris units were then traced up-glacier to their source area and lithology identified using the regional geological map produced by Searle et al. (2010). Spectra from 200 pixels were then compared to spectra from the USGS spectral library in ENVI to confirm correct classification. 91% of sampled pixels were correctly classified based on these independent data. Mass movement deposits were identified by the presence of two features: a scar, identified as an elongate feature on the valley side which differed in colour to the surrounding valley wall, suggesting erosion and loss of vegetation had occurred, and an associated lobate debris fan deposit on or near the glacier surface. A Normal Difference Water Index (NDWI) was used to identify pixels containing supraglacial water, calculated from ASTER bands 3 (Near Infrared; NIR) and 4 (Shortwave Infrared: SWIR) after (Gao, 1996):

$$NDWI = (NIR\ (Band\ 3) - SWIR\ (Band\ 4))/\ (NIR\ (Band\ 3) + SWIR\ (Band\ 4)) \qquad (2)$$

The classification of water was verified through manual comparison of 100 randomly selected features classified as water in the 2011 ASTER imagery with high resolution (2.5 m) Quickbird imagery from 2011 for the same locations. All 100 features were identified as water in both images, and so were assumed to be correctly classified. The area of debris units and supraglacial water bodies were derived using the geometry calculator in ArcGIS (v.10.1).

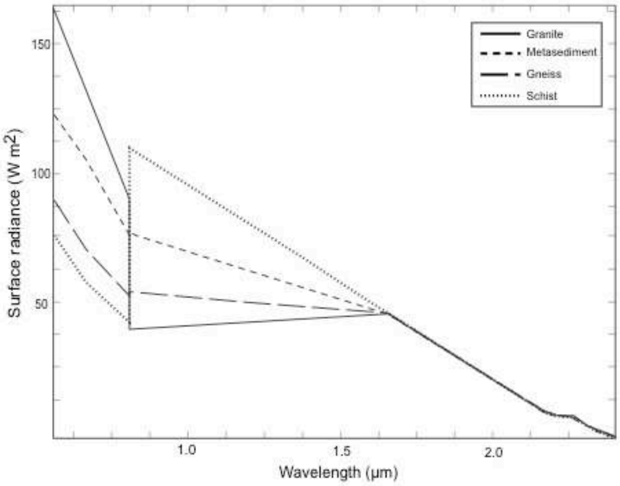

Figure 2: Spectral reflectance profiles for the different lithology types identified on Baltoro Glacier.

3.3. Sediment flux

Supraglacial sediment flux across the glacier surface was calculated using derived debris thickness and surface velocity data, following the method developed by Heimsath and McGlynn (2008) to determine headwall retreat rate on Milarepa's Glacier in Nepal. Heimsath and McGlynn (2008) measured debris thickness and surface velocity along one transect near the glacier headwall, then calculated cross-sectional area of the debris using the debris thickness transect, and multiplied the cross-sectional area by surface velocity, calculating one-dimensional sediment flux. Here, we calculated supraglacial sediment flux for each pixel by multiplying debris thickness by the pixel width at right angles to the direction of maximum surface velocity to give supraglacial debris layer cross-sectional area, and then multiplied cross-sectional area by surface velocity for the same pixel. As surface velocity and supraglacial debris thickness were used to calculate sediment flux these results only represent debris transported supraglacially. The resulting sediment flux maps were normalized to annual datasets to obtain comparable sediment flux values, and were masked using the same masks applied to the surface velocity and debris thickness maps to exclude pixels with erroneous results and cloud cover.

4. Results

4.1. Debris thickness

A similar pattern of debris thickness distribution was present in 2001, 2004 and 2012 (Figure 3). In the upper section of the glacier above and around Concordia, debris was distributed in alternating bands of thicker debris (around 0.2–0.3 m thick) and thin, sparsely-distributed or non-existent debris layers (≤ 0.02 m), in a longitudinal pattern parallel to ice flow. Thicker bands of debris originated from the glacier margin, primarily at confluences between tributary glaciers and the main glacier tongue, which were interpreted to be medial moraines. In the glacier mid-section, debris coverage became increasingly spatially extensive with decreasing distance from the glacier tongue, and a general thickening of debris towards the glacier terminus occurred. No build up of debris, such as that expected where a terminal moraine is present, was observed at the glacier terminus from satellite data, confirming the absence of such a feature previously observed in the field by Desio (1954). Debris covered the entire glacier surface in the lower section of the glacier and was predominantly > 0.5 m thick.

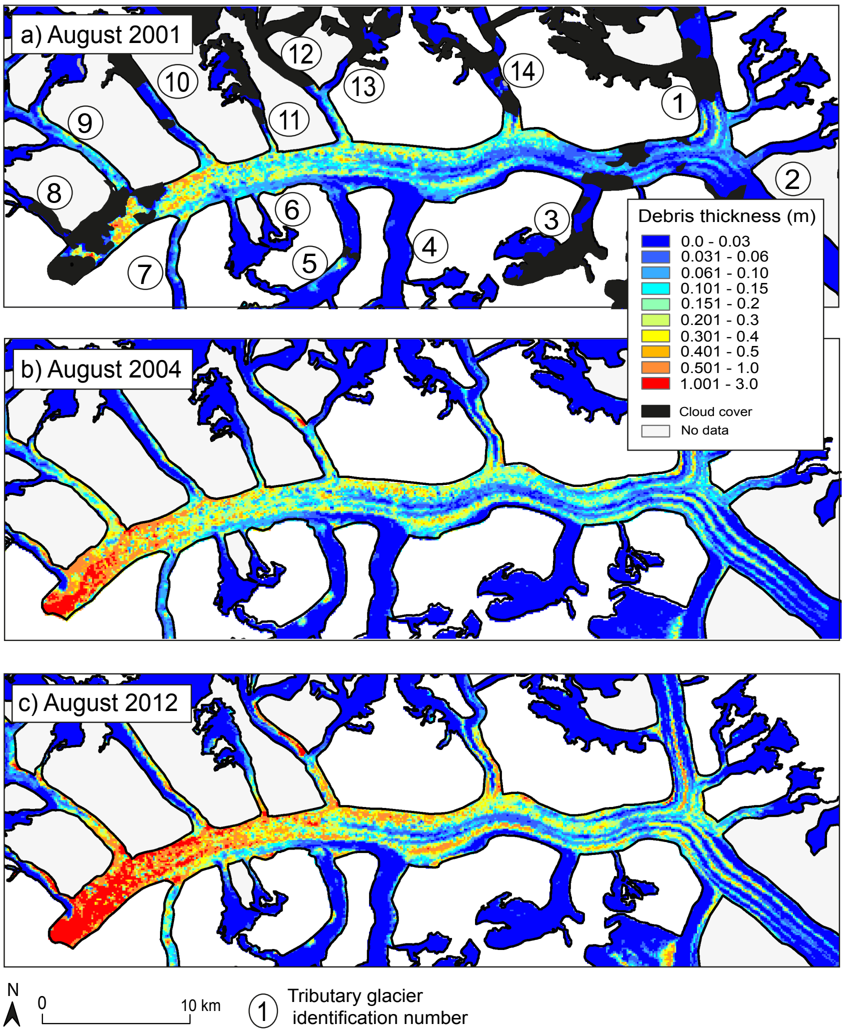

Figure 3: Debris thickness maps of Baltoro Glacier for: (a) August 2001; (b) August 2004; (c) August 2012.

The broad, glacier-wide pattern of debris distribution displayed minimal change between 2001 and 2012, suggesting that a pattern of debris input and transport was already established across the glacier and persisted over the study period. However, the thickness of the debris layers across the glacier varied over the 11-year study period. Cloud cover in 2001 restricted comparison between 2001 and 2004 in the glacier's lower section, but thickening of the medial moraines in the glacier upper-section of the order of around 0.1m was seen during this 3-year time period. A general trend of increasing debris thickness in the glacier mid-section was seen between 2001 and 2012, with a mean debris layer thickness in the glacier mid-section of ~0.28 m in 2001, ~0.34 m in 2004 and ~0.41 m in 2012. Debris thickness was most variable in the glacier lower section between 2004 and 2012, with a mean debris layer thickness of ~0.71 m in 2004 and ~1.5 m in 2012, and an apparent thickening of debris at the terminus, although further field data would be needed to confirm these mean debris thicknesses due to the independence of debris surface temperature with debris layer thickness above 0.5 m. Increasing debris thickness in the lower and mid sections suggests a progressive backing up of debris through time causing the area of thickest debris to increase up-glacier from the terminus.

In 2004 a sharp boundary between debris layer thicknesses was observed running longitudinally from the glacier terminus to the location at which Trango Glacier (Tributary Glacier 9) joins the main glacier tongue (Figures 1b; 3). South of the boundary debris thickness was above 0.5 m thick, whilst north of the boundary debris layer thickness was less than 0.5 m thick. The debris thickness boundary correlates with the boundary between a granite debris unit originating on Trango Glacier and gneiss debris units of the main glacier tongue, presumed to also be the boundary between the main glacier flow units and Trango Glacier flow unit.

4.2. Glacier surface velocity

A general trend of highest velocity at Concordia, where Baltoro South and Godwin-Austen Glacier converge, and subsequently decreasing surface velocity down-glacier of Concordia towards the terminus was observed at all time periods, with very low (less than 20 m a^{-1}) to no glacier flow near the terminus (Figure 4). Variations in surface velocity occurred between 2001 and 2012, with an average decrease in surface velocity of around 50 m a^{-1} along the longitudinal profile of the glacier (Figure 4a) between 2001 and 2004, followed by an increase on the same order of magnitude between 2004 and 2012 (Figure 4d). Higher surface velocities were observed at Concordia where the Godwin-Austen and Baltoro South Glaciers join, and subtle velocity increases at some but not all tributary glacier confluences were also noted (e.g. Yermanendu and Mandu glaciers; Tributary glaciers 4 and 5, respectively). In 2012 glacier surface velocity was lowest (~0–20 m a^{-1}) in the northwest region of the terminus, a triangular shaped area which extended from the glacier terminus and pinched out at around 5 km up-glacier of the terminus and downstream of Trango Glacier. However, in 2004 no such pattern was evident and a patchy distribution of velocity between 0 and 50 m a^{-1} across the glacier width for around 10 km up-glacier of the terminus occurred.

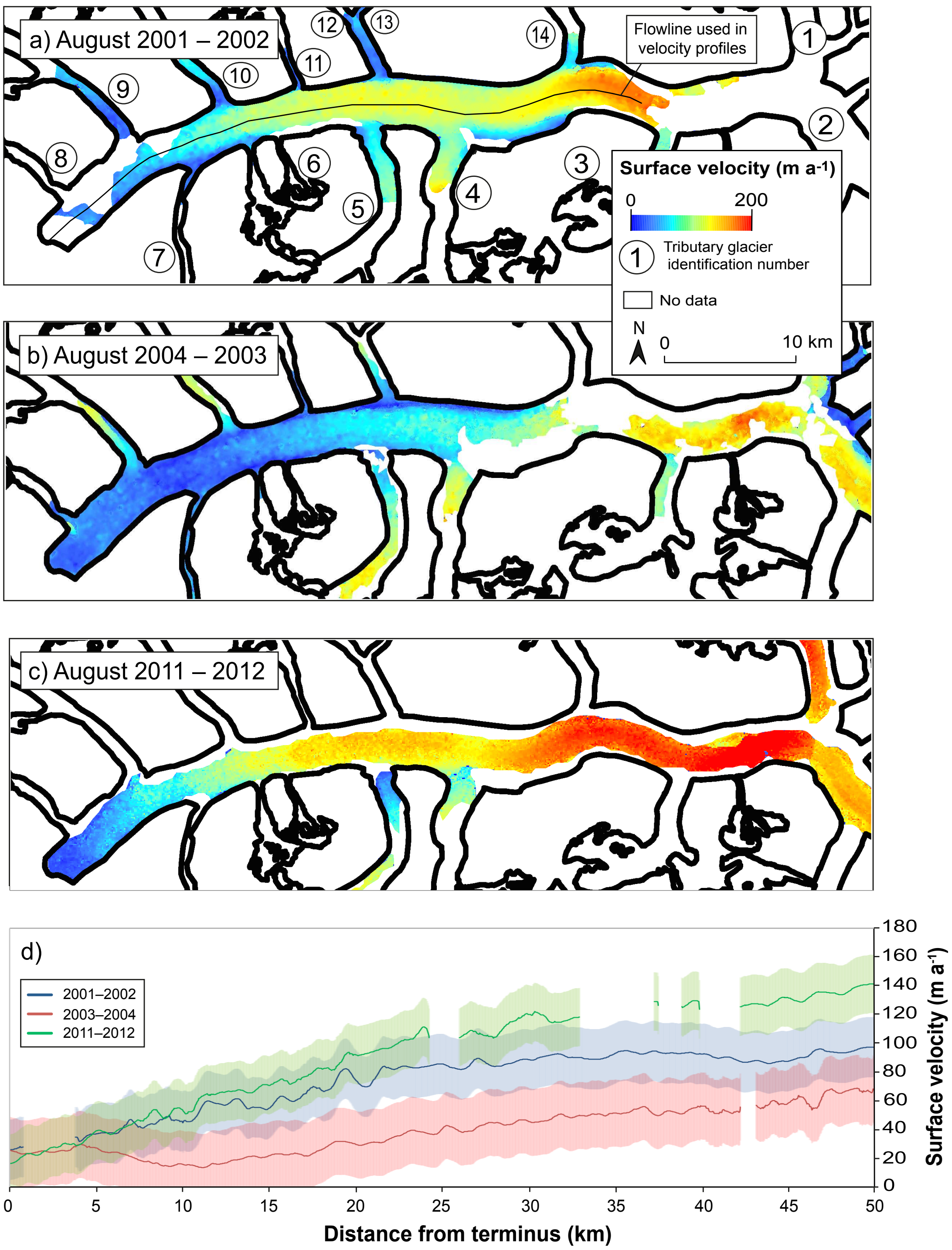

Figure 4: Surface velocity maps in m a^{-1} for Baltoro Glacier for: (a) 2001, (b) 2004 and (c) 2012, and (d) surface velocity profiles along the centre line of the main glacier tongue with uncertainty values of each velocity line displayed with shaded regions.

4.3. Geomorphological features

Supraglacial debris lithology was identified through comparison of ASTER pixel spectra with spectra of lithologies from the USGS spectral library and with reference to the geology map produced by Searle et al. (2010). The supraglacial debris on Baltoro Glacier was dominated by gneiss (~51–53 % of the debris-covered glacier area), whilst ~47–49 % was composed of granite (~27 %), schist (~12 %) and a small proportion of metasediment (~6 %) (Figure 5, Table 3). Across the main glacier tongue, negligible change in debris unit boundaries occurred between 2001 and 2012 and change in percentage cover of debris units was attributed to errors produced by manual digitisations (Gibson et al., 2016; Table 3). However, small scale variations in debris distribution did occur on tributary glaciers between 2001 and 2012, which have been attributed to these glaciers being in various periods of instability, possibly related to surge phases,, and input of debris material from surrounding valley walls through rock- and snow avalanches (Gibson et al., 2016). For example, patches of thicker debris on Mandu Glacier (Tributary Glacier 5) can be tracked down-glacier between 2001 and 2012 in geomorphological maps (Figure 6d) and debris thickness maps (Figure 6e), with debris initially deposited on the glacier by a mass movement event and then transported as a bulk volume.

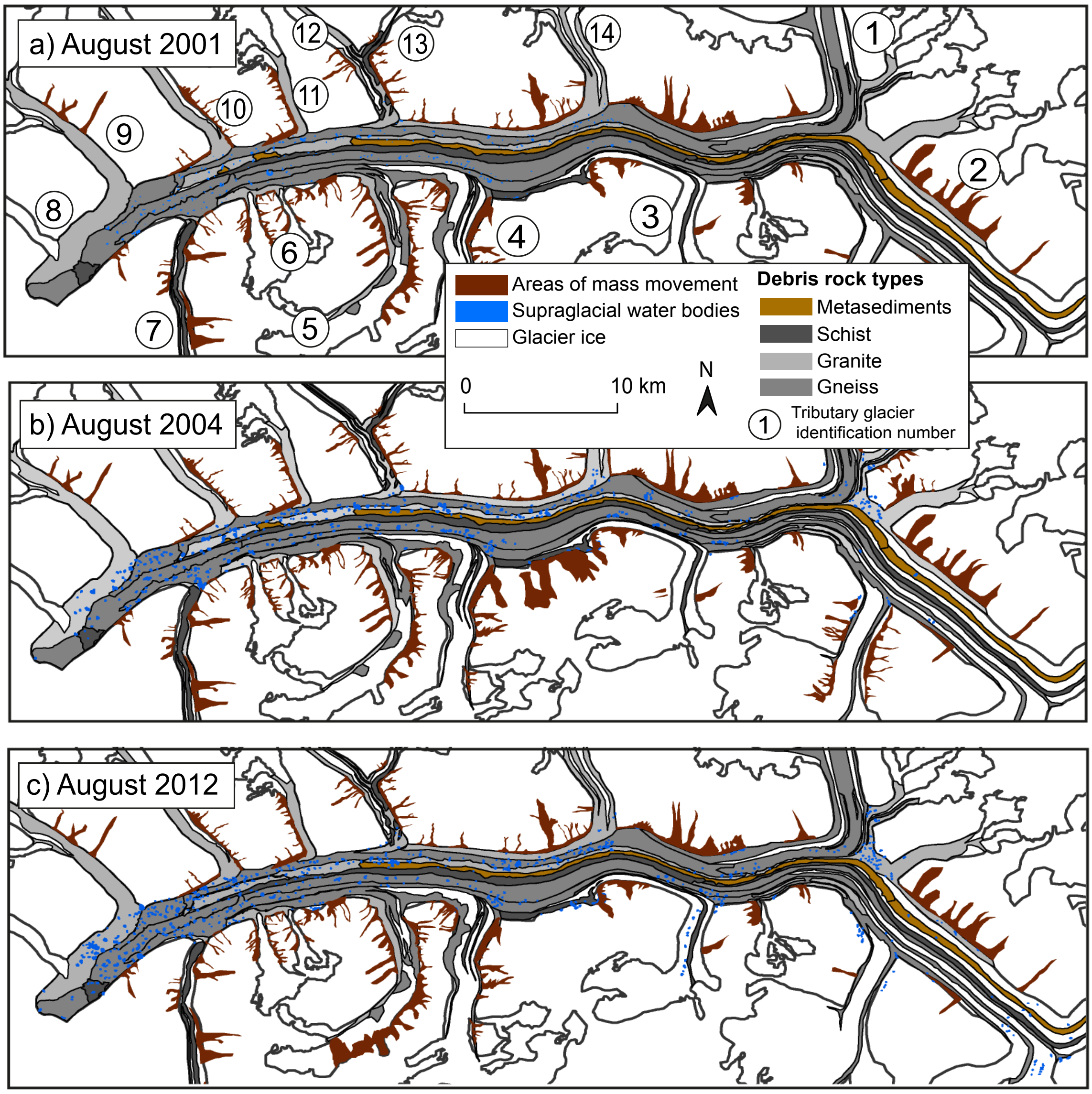

Figure 5: The surface geomorphology of Baltoro Glacier in (a) August 2001, (b) August 2004 and (c) August 2012.

Table 3. Total area of each debris unit type, based on lithology, for 2001, 2004 and 2012, and the percentage of each debris type as a proportion of the total debris cover for Baltoro Glacier and its tributary glaciers (Gibson et al., 2016). Variability in total debris area is attributed uncertainty produced by manual digitisation.

Year	**2001**	**2001**	**2004**	**2004**	**2012**	**2012**
Debris type	**Area (km^2)**	**% of total debris**	**Area (km^2)**	**% of total debris**	**Area (km^2)**	**% of total debris**
Gneiss	81.48	52.9	79.83	51.2	79.48	52.9
Metasediment	8.60	5.6	11.41	7.3	8.28	5.5
Schist	17.76	11.5	18.54	11.9	17.71	11.8
Granite	46.29	30.0	46.20	29.6	44.71	29.8
Total debris (km^2)	154.13		155.97		150.17	

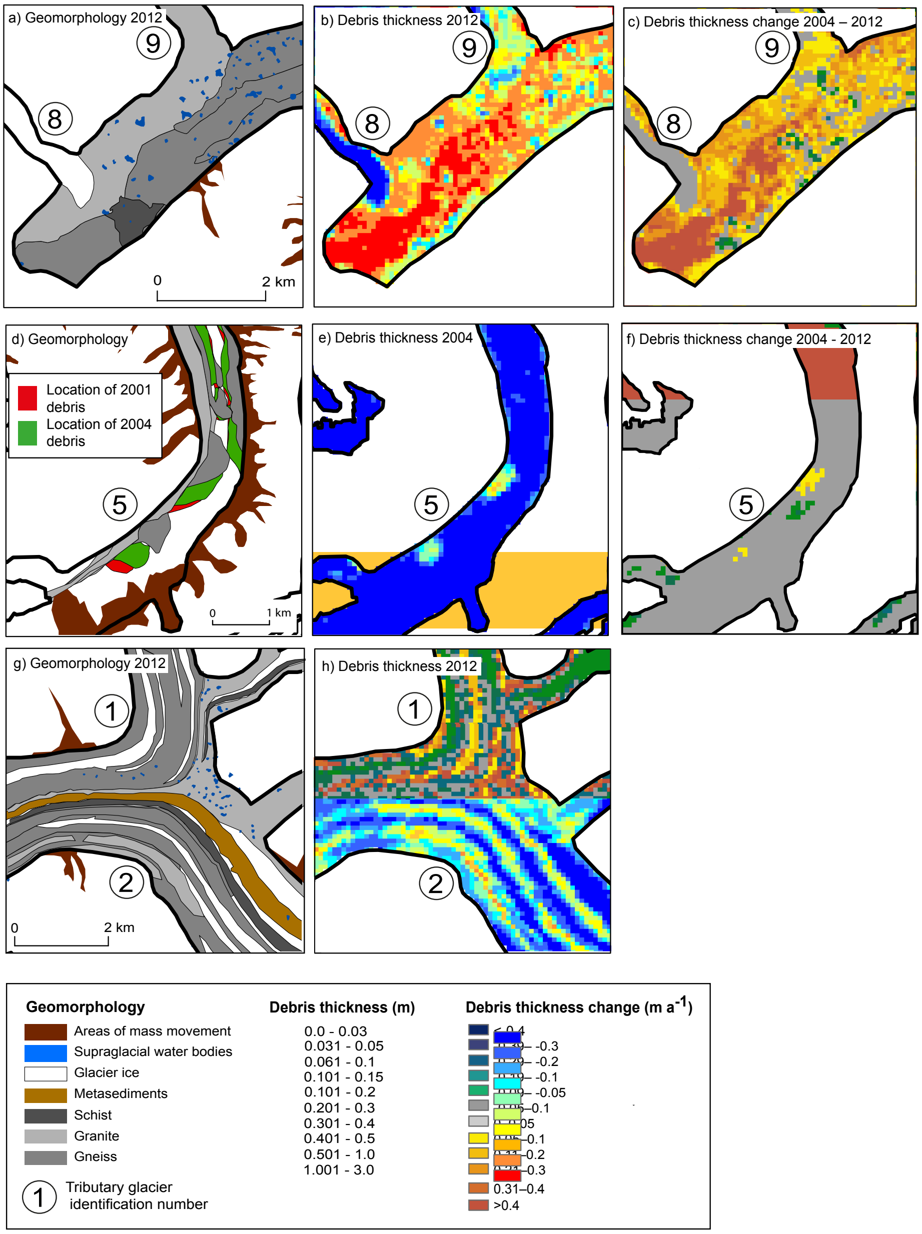

Figure 6: Comparison of: (a) geomorphology, (b) debris thickness and, (c) debris thickness change at the terminus of Baltoro Glacier, showing a distinct boundary between debris thickness values and debris units of different lithologies; (d) geomorphology, with previous positions on areas of supraglacial debris from 2001 (red) and 2004 (green) displayed, (e) debris thickness and (f) debris thickness change on Mandu Glacier (Tributary Glacier 5) showing the down-glacier movement of debris pockets through time; (g) geomorphology and (h) debris thickness of the confluence area between Godwin-Austen Glacier and Baltoro South Glacier in 2012, showing an area of thick debris up-glacier of where the tributary glaciers join and change direction to form the main glacier tongue.

Supraglacial water bodies occurred most frequently in the lower to lower-mid-sections of the glacier between 2001 and 2012, and in areas of relatively thick debris, such as east of the confluence between Goodwin-Austen and Baltoro South Glaciers (Figure 6g and 6h). However, at all time points an absence of supraglacial water bodies was present in the gneiss debris unit at the terminus of the main glacier tongue and around the terminus of Tributary Glacier 8 (unnamed). The number of supraglacial water bodies increased by 336 over the study period, from 234 in 2001 to 570 in 2012 (Table 4). Total area of supraglacial water bodies increased by almost 400 % during the same period. Temporally, the greatest change in water body number and area occurred between 2001 and 2004, whilst spatially the greatest increase in water body number occurred in the lower mid-section and east of Concordia at up-glacier margin of the confluence between Godwin-Austen and Baltoro South Glacier.

Table 4. Supraglacial water area and number on Baltoro Glacier in 2001, 2004 and 2012 (Gibson et al., 2016).

	2001	**2004**	**2012**
Number of water bodies	234	404	570
Area (km^2)	0.66	1.79	2.04

4.4. Annual debris thickness change

Mean annual debris thickness change (Figure 7) showed areas of debris thickness increase predominantly occurred in the lower section of the glacier and along medial moraines, and were of the order of 0.05 to 0.3 m a^{-1}, greater than uncertainty values for debris thickness maps. In areas of decreasing debris thickness a reduction in thickness of the order of 0.05–0.09 m a^{-1} was observed, with most change occurring between 2001 and 2004, although these areas of decrease were lower than the uncertainty values associated with the debris thickness maps. Such areas of decreasing debris thickness occurred on the northern margin of the main glacier tongue and parallel to debris layer thickening of medial moraines. Debris thickening occurred at a similar rate and pattern in the lower section of the glacier between the two periods, with the greatest increase along the boundary between the main glacier tongue and Trango Glacier (Section 4.1). During both periods, increase in debris thickness was primarily along the moraine crests in the mid-section of the glacier, with more extensive increases between 2001 and 2004, extending to the glacier upper-section. Debris thickness change on tributary glaciers was of the order of ±0.05 m a^{-1}, with specific areas of debris change apparent, including deposits on Mandu Glacier, considered to have been derived from mass movement events which moved down-glacier through time, revealed through a loss of thickness in their previous position and an increasing debris thickness in the current position (Figure 6f).

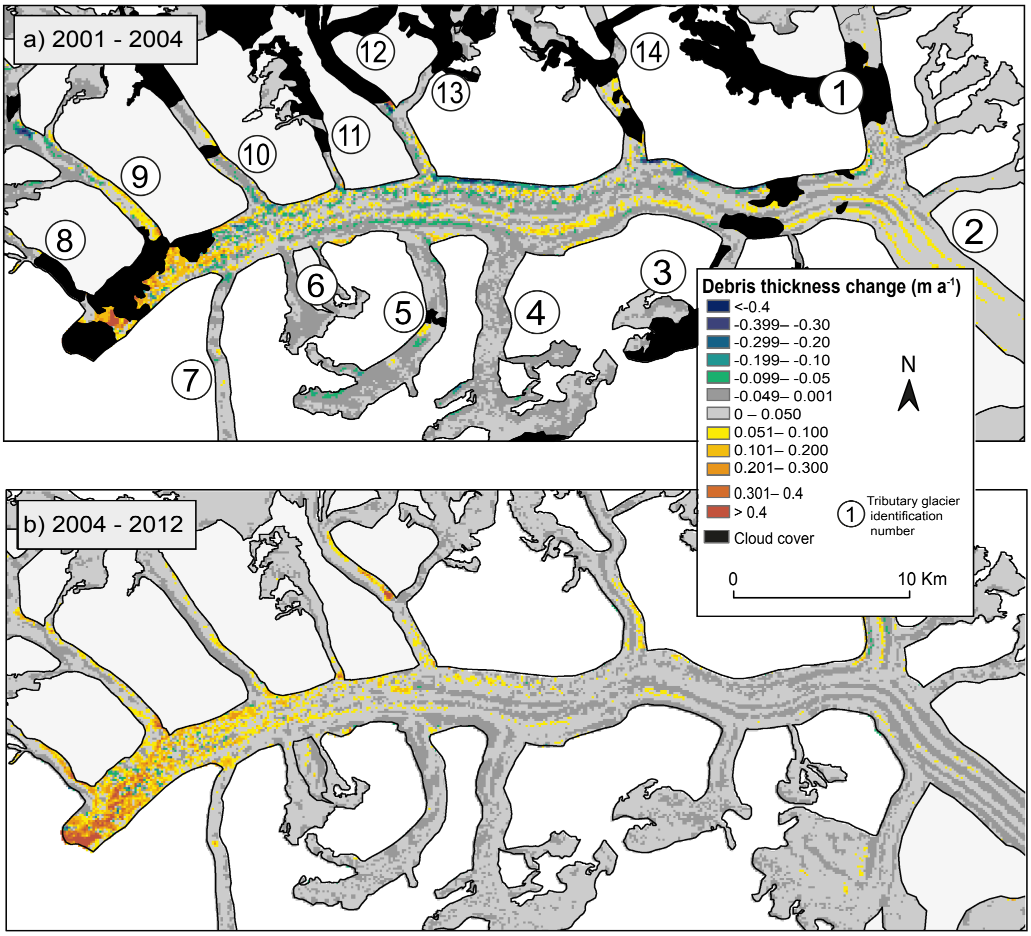

Figure 7: Annual debris thickness change, calculated by subtracting the earlier debris thickness map from the later, and then divided by the number of years between the two maps, for (a) 2001 – 2004 and (b) 2004 – 2012.

4.5. Annual sediment flux

Supraglacial sediment flux (Figure 8) showed a similar spatial distribution for all points in time, with the highest sediment flux (between 11000 and 12000 m^3 a^{-1}) in the lower section of the glacier and along the northern glacier margin in the glacier mid-section. Areas of higher sediment flux (>9000 m^3 a^{-1}) were also found at the confluence of tributary glaciers and the main glacier tongue, such as east of Concordia (2003-2004), Yermanendu Glacier (Tributary Glacier 4; 2001-2002) and Tributary Glacier 6 (unnamed; 2001-2002, 2003-

2004). For a large proportion of the mid- and upper sections of the glacier, sediment flux was generally less than 1000 m^3 a^{-1}, with some areas of relatively higher sediment flux along moraine features (4000–6000 m^3 a^{-1}).

A general pattern of increasing sediment flux was seen between 2001–2002 and 2011–2012 along medial moraines in the lower section of the glacier, with an increase in sediment flux on the order of between 5000–6000 m^3 a^{-1} between 2001 and 2002 to 6000–8000 m^3 a^{-1} between 2001 and 2012. In the upper-mid and upper-sections of the glacier these medial moraines had a constant sediment flux of around 6000 m^3 a^{-1}. Although the sediment flux maps do not extend to the initiation point of many of the medial moraines where debris is introduced into the upper glacier system, consistency in sediment flux along moraine features suggest input from valley wall erosion and entrainment was stable over the sub-decadal period. In the 2001–2002 and 2003–2004 sediment flux maps pockets of sediment flux less than 1000 m^3 a^{-1} in the lower section of the glacier corresponded to the location of supraglacial water bodies.

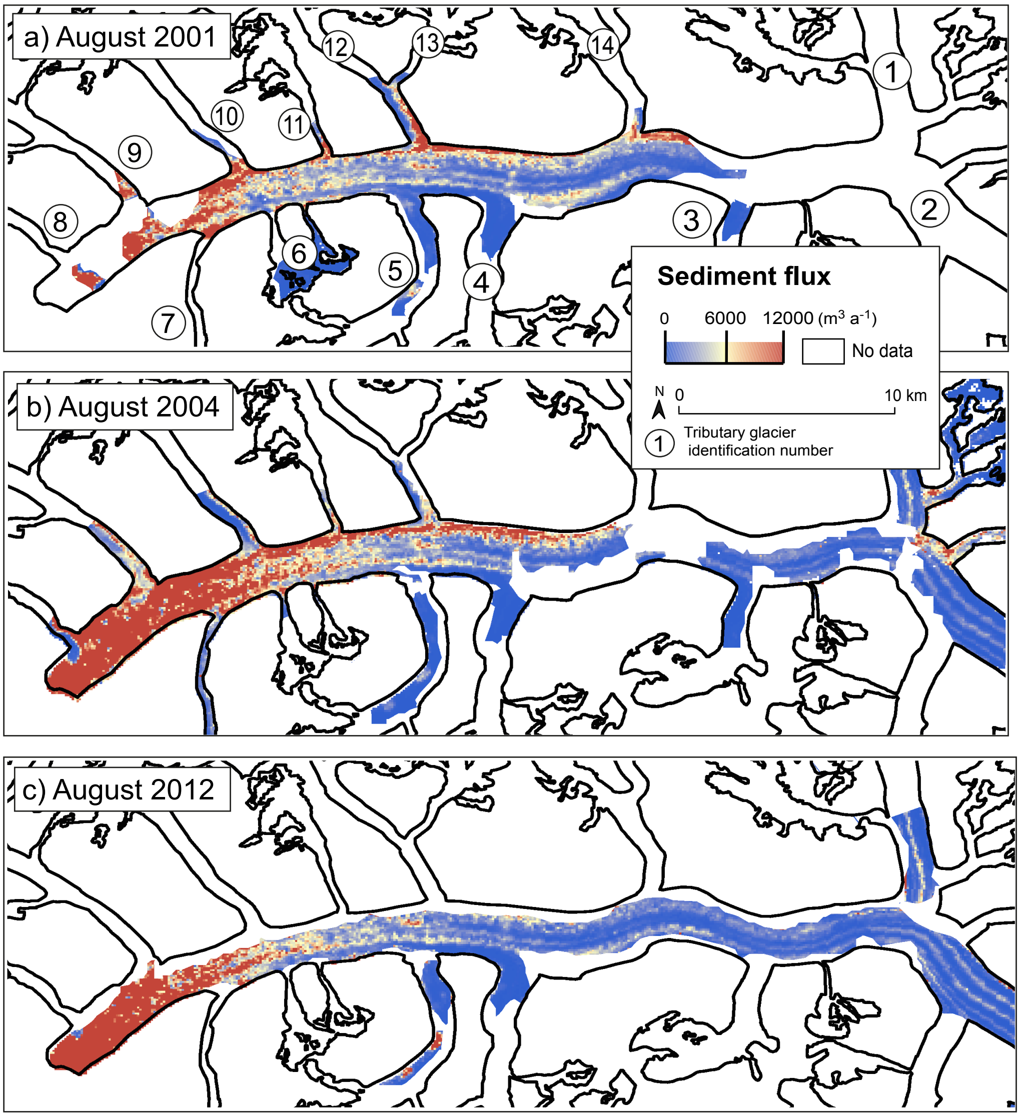

Figure 8: Sediment flux; debris cross-sectional area for each pixel multiplied by surface velocity, for (a) 2001–2002, (b) 2003–2004 and (c) 2011–2012.

5. Discussion

5.1. Spatiotemporal change in supraglacial debris distribution

A debris distribution common to the majority of debris-covered glaciers is evident on the surface of Baltoro Glacier throughout the study period, with the thickest debris occurring near the terminus and along moraine crests, and an increasingly thick debris layer towards the terminus (e.g. Figure 9; Fushimi et al., 1980; Kirkbride and Warren, 1999; Mihalcea et al., 2006b; Zhang et al., 2011). A progressive increase in the area covered by debris through time would be expected due to debris being constantly transported to the glacier terminus; such a pattern is observed on Baltoro Glacier between 2001 and 2012, and combined with continued glacier flow would result in a build-up of debris in the lower sections (Kirkbride and Warren, 1999), particularly where there is no efficient sediment evacuation down-valley. A mean increase in debris thickness of between 0.05 and 0.10 m across the glacier surface occurred during the study period. Where the debris layer is below 0.5 m, the thickness at which ablation of underlying ice is most variable with debris thickness, the rate of debris thickness change identified here could lead to areas of the debris layer evolving from a thickness that enhances melt to one that insulates it over relatively short timescales (e.g. several years). The rapidity of such changes could render debris thickness maps previously published to be inapplicable for any year other than the one in which debris surface temperature data were collected (e.g. Mihalcea et al., 2008), although such maps would still be important for observing historical debris distribution.

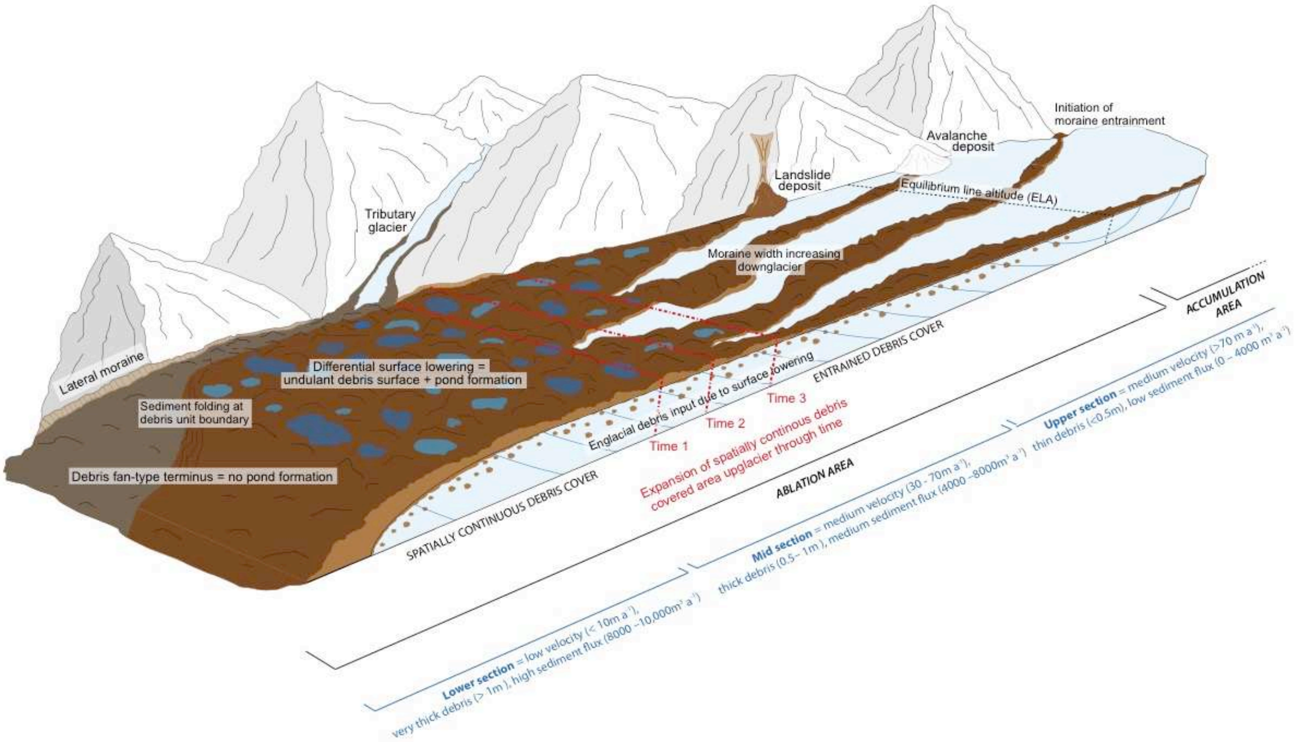

Figure 9: Schematic diagram of a debris-covered glacier system with input, transport and depositional processes alongside glacier dynamics for each section of the glacier, and the change in debris-covered area through time (T_1–T_3).

Debris thickness change in the lower- and mid-sections of Baltoro Glacier is attributed to a combination of differential surface ablation resulting in debris shift between topographic highs and lows, collapse of medial moraines, and redistribution of debris following input from mass movement events, all processes that commonly occur on debris-covered glaciers (e.g. Anderson and Anderson, 2016; Hambrey et al., 1999; Hambrey et al., 2008; Heimsath and McGlynn, 2008). The presence of a sharp change in debris thickness between the main glacier tongue and Tango Glacier is attributed to variations in relative surface velocity between the two flow units and the subsequent entrainment along flow unit boundaries. In high resolution Quickbird imagery (accessed from Google Earth (2017) on 16/01/17) a ridge at the boundary between the main glacier tongue and Trango Glacier flow units is observed, which has been mapped alongside other glaciological features such as sediment folds and ogives (Figure 10). The ridge extends from the bedrock at the up-glacier confluence between the two debris units (Figure 10a), suggesting the ridge is a medial moraine between the two flow units. Parallel to the supraglacial debris ridge are a series of deformation structures in the debris cover (Figure 10a), attributed to progressive supply and subsequent compression of debris through time as continuation of flow of the main glacier flow unit towards the terminus is constricted and blocked by the incoming flow unit of Trango Glacier. Variation in debris distribution near the terminus is further complicated by Trango Glacier displaying signs of a period of dynamic instability prior to the study period, with increasingly sinuous moraines on its surface through time (Figure 10a) and propagation of an area of high velocity along the tributary glacier's length between 2001 and 2004 (Figure 5). These geomorphological features alongside the temporal pattern observed on the glacier over the study period are consistent with a glacier that may have undergone a surge event, or at least a change in relative velocity to the ice flow unit it interacts with (Meir and Post, 1969). An arc of granitic debris that mirrors the terminus shape of Tributary Glacier 8 appears to suggest that this glacier is also dynamically linked to the terminus (Figure 10a). These geomorphological patterns suggest the main debris units were transported and deposited prior to input of debris from Tributary Glacier 8 and Trango Glacier, and indicate that initiation of debris supply along the main glacier and tributary glaciers were not contemporaneous.

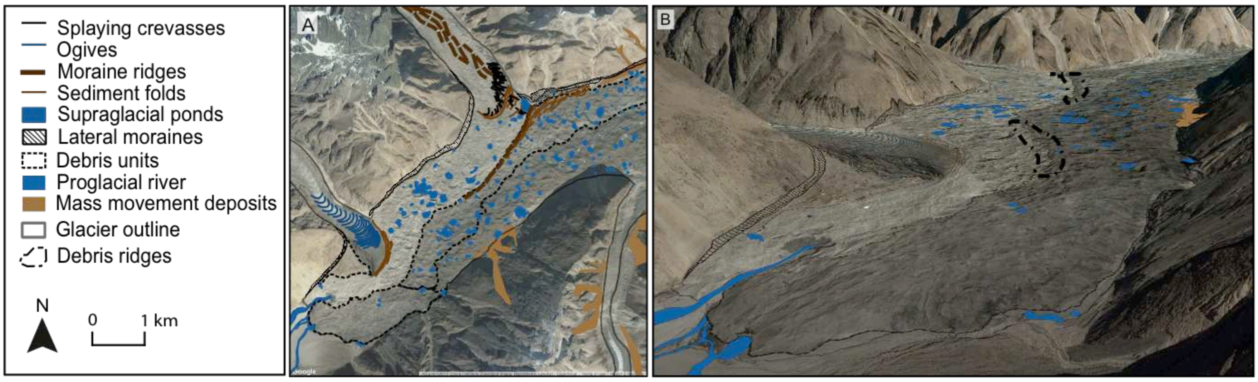

Figure 10: A (a) geomorphological map and (b) annotated oblique Quickbird image displaying the moraine ridge structure and associated sediment folds at the boundary between Trango Glacier (Tributary glacier 9) and the main glacier tongue, and the difference in debris lithology between the two glaciers. Accessed from Google Earth (2017) on 16/01/17.

5.2. Processes controlling debris distribution

Sustained debris thickening between 2001, 2004 and 2012 was observed, although notable spatial variability exists. Sediment flux also appeared to be temporally constant across much of the glacier despite variations in surface velocity, although some small-scale variations in sediment flux did occur. Changes in sediment flux in the lower section of the glacier were considered to be a product of increasing debris thickness near the terminus and sustained surface velocity as more debris was delivered to the slow-flowing terminus area through time. Variation in sediment flux between 2001–2002 and 2003–2004 in the glacier mid-section, south of Dunge and Biale Glaciers (Tributary Glaciers 10 and 11), are attributed to a combination of increasing debris thickness and increasing area of thicker debris up-glacier of the terminus and to an increase in surface velocity, as sediment flux varied considerably in this region between the two periods despite a lack of time separation. However, the overall glacier-wide stability in the rate of debris thickening and the pattern of sediment flux suggests that supraglacial debris transport was not the sole control of spatiotemporal changes in debris layer thickening. In periods of higher velocity (e.g. 2011–2012) it is likely that less debris built up on the glacier surface prior to transportation, causing a thinner layer of debris to be transported down-glacier than in previous years, albeit at a faster rate, and vice versa for periods of low velocity. Variability in surface velocity and its influence on debris transport is particularly pertinent for Baltoro Glacier, where velocity has been found to vary from year to year, observed here and by Quincey et al. (2009). Longer term studies (of the order of a number of decades) considering the interaction between surface velocity and debris distribution are needed to determine the relationship of these two parameters over decadal to centurial timescales. Consequently, the rate of debris input over sub-decadal timescales is thought to control temporal variations in debris layer thickening across the glacier. Over sub-decadal timescales, debris input will vary as a result of the frequency of mass movement events, which would significantly increase local supraglacial debris volume and affect velocity if the volume was great enough (e.g. Tovar et al., 2008). Over longer timescales (>100 years) debris input would be controlled by regional erosion rates, which are in turn controlled by climatic conditions, most notably precipitation, and tectonics, including rates of uplift and deformation in active tectonic regions such as the Karakoram (Molnar et al., 2007; Scherler, 2014). Regional erosion rates therefore control the long-term (centurial to millennial) rates of debris input to a glacier system, but over shorter (sub-decadal) periods the frequency and location of mass movement events are important controls on spatiotemporal variations in supraglacial debris distribution.

The total area and number of supraglacial water bodies increased between 2001 and 2012, and temporal changes in these parameters were notably larger than the uncertainty involved in incorrect classification of pixels containing water. The greatest percentage change in supraglacial water body number (73 %) and area (171 %) occurred between 2001 and 2004. Increase in supraglacial water body area and number has previously been attributed to changes in precipitation since 2000 (Quincey et al., 2009; Gibson et al., 2016). However, increasing supraglacial water body frequency on debris-covered glaciers is often considered analogous with stagnation and surface lowering of debris-covered glaciers (e.g. Sakai et al., 2000). Such differential surface lowering forms the undulating debris topography, which then promotes the formation of supraglacial water bodies (Hambrey et al., 2008). Since 2004, Baltoro Glacier has showed no sign of stagnation but has undergone surface lowering of the order of 40 m between 2000 and 2008 (Gardelle et al., 2012). Such surface lowering is apparent up-glacier of the confluence between Trango Glacier and the main glacier tongue, where the debris surface displays a high density of topographic highs and depressions (Figure 10). Surface lowering of some glaciers in the Karakoram has been attributed to negative mass balance of glaciers in response to recent climatic change (Gardelle et al., 2012), although in the case of Baltoro Glacier it could equally be a consequence of its tributary glaciers being in various phases of dynamic instability. Glacier dynamic instability would cause temporal variation in ice flux to the main glacier tongue. Following the end of these phases of dynamic instability, ice mass delivery to the main glacier tongue would reduce, causing temporary reduction in surface velocity, as observed between 2001 and 2004 on Trango Glacier, and thus surface lowering. To understand the relative controls of climatic change and dynamic instability of tributary glaciers on surface velocity and lowering of Baltoro Glacier longer-term records of surface lowering, a greater record of glacier mass balance and localised meteorological data are needed.

Debris thickness maps presented here show no evidence for a thicker accumulation of debris at the glacier terminal margin, the presence of which has previously been interpreted as a terminal moraine on maps of debris thickness for topographically confined glaciers such as Khumbu Glacier in Nepal (Rounce and McKinney, 2014; Rowan et al., 2015; Soncini et al., 2016). Baltoro Glacier is thought to lack such a terminal moraine due to the glacier being of debris-fan-type, the occurrence of which is linked to glaciers located in wide, gently sloping valleys (Kirkbride, 2000). Debris-fan termini have a steeply sloped topography relative to the near horizontal glacier surface up-glacier of the terminus. The presence of a sloped debris surface suggests the same is true for the underlying ice surface (e.g. Figure 9), both of which would facilitate more efficient supra- and englacial drainage systems and inhibit the formation of undulating topography in the supraglacial debris layer near the terminus, as debris will be less stable and is more likely to be transported more evenly when located on a slope. The lack of depressions near the glacier terminus would therefore inhibit ponding of supraglacial water in the area.

5.3. Incorporating debris distribution change into numerical modelling

Mean annual debris thickness change and mean annual sediment flux are potential indicators to help establish the period over which a glacier has become debris covered and the rate at which supraglacial debris layers evolve. Currently in numerical models of debris-covered glaciers debris thickness is largely considered as static in time (e.g. Collier et al., 2014; Reid and Brock, 2010; Shea et al., 2015). However, we have confirmed debris distribution is dynamic over annual to decadal timescales (Figure 3; Figure 9). Incorporating an annual rate of debris thickness change into long-term energy balance models for debris-covered glacier surfaces is therefore important for generating robust results using these methods. For glacier change models, such as those of Rowan et al. (2015), where a supraglacial debris layer is formed through glacial processes and hillslope erosion rates are used to control input of debris to a glacier system, annual rates of glacier change and sediment flux could be used to constrain model outputs. We also confirm that using temporally constant annual erosion rates for control of debris input to glacier systems, such as those used by Rowan et al. (2015) and Anderson and Anderson (2016), is appropriate on sub-decadal timescales, but should be set on a case by case basis as these erosion rates would be affected by localised variability in headwall retreat and precipitation (Bookhagen et al., 2005; Pan et al., 2010). For longer-term studies the effect of a changing climate should be considered in regional erosion rates used for such numerical models (Peizhen et al., 2001; Scherler, 2014). Additionally, the rate of debris layer thickness change is likely to vary between glaciers due to varying input of debris, glacier size, landscape, climate and bedrock lithology, and needs to be evaluated for individual cases.

To accurately determine the formation and evolution of a supraglacial debris layer a greater understanding of the volume of debris contributed from englacial debris input and the role varying ice velocity with depth plays in englacial debris transport is needed. At present, calculation of englacial debris meltout has not been attempted in great detail (e.g. Rowan et al., 2015; Anderson and Anderson, 2016). Recent work on debris-covered glaciers has highlighted rockfall in accumulation areas can be incorporated rapidly to englacial locations (Dunning et al., 2015), but very little is known regarding the volume of debris contained within the glacier ice of debris-covered glaciers (Anderson 2000). Enhanced ablation and surface lowering, as seen on Baltoro Glacier from the start of the 21st century (Gardelle et al., 2012) is likely to result in an increased rate of debris meltout (Bolch et al., 2008; Kirkbride and Deline, 2013). By quantifying the volume of debris contributed to a glacier surface through englacial meltout a more comprehensive understanding of processes by which debris distribution is controlled, both through space and time, could be gained. Such data have previously been collected through the use of ground penetrating radar (e.g. McCarthy et al., 2017), but a greater spatial coverage of such data across glacier surfaces is needed to understand spatial variability in englacial debris distribution.

6. Conclusion

The distribution of supraglacial debris on Baltoro Glacier predominantly follows the expected pattern for a debris-covered glacier, with increasingly thick debris towards the terminus. However, debris distribution is complicated by the interaction between tributary glaciers, some of which show signs of dynamic instability, and the main glacier tongue. An overall increase in debris thickness was observed between 2001 and 2012, indicating that supraglacial debris distribution varies over sub-decadal timescales. Short-term variations in debris thickness are primarily attributed to input from mass movement events. The area of Baltoro Glacier covered by a spatially continuous debris layer increased over the study period, suggesting that the debris layer is still evolving. The number and area of supraglacial water bodies on Baltoro Glacier also increased through the study period, with changes attributed to differential surface lowering. However, ponding is not observed at the terminus because the glacier displays a debris-fan type terminus that inhibits formation of undulating debris topography and facilitates efficient drainage. Additionally, surface lowering of the glacier surface up-glacier of the terminus may be important for debris layer thickening due to exhumation of debris transported englacially.

Quantifying the influence of mass movement deposits and englacial meltout on supraglacial debris distribution is important to better understand the evolution of debris-covered glaciers through time, particularly to determine the mass balance of glaciers accurately in response to recent and future climatic change. However, quantifying such inputs is challenging; mass movement events are temporally and spatially variable and dependant on climate, topography, tectonic processes and lithology, and identifying debris contributed from englacial sources requires quantification of the volume of debris held englacially, which can only really be gained through fieldwork. Despite such limitations, this study shows that incorporating some aspects of spatiotemporal change in supraglacial debris distribution into numerical modelling is achievable, and is likely to be significant in accurately determining debris-covered glacier systems.

Acknowledgements

The authors would like to thank NASA and Google for free access to ASTER and Quickbird imagery, which made this study possible. We would also like to thank Dr. Simon Cook and an anonymous reviewer for their thorough and constructive reviews of the manuscript.

Author contributions

Morgan Gibson – conceived the study, carried out the data processing and analysis and wrote the manuscript.

Neil Glasser – contributed to data analysis and refinement of discussion

Duncan Quincey – contributed to data analysis and final editing of the manuscript

Ann Rowan – contributed to idea development and final editing of the manuscript

Christoph Mayer – collection of field data, contributed to data analysis and refinement of discussion

Tristram Irvine-Fynn – contribution to wording in the introduction and discussion of the manuscript, and editing of the manuscript.

References

Abrams, M., Hook, S. and Ramachandran, B., 2002. ASTER User Handbook, v. 2. Jet propulsion laboratory, Californian Institute of Technology. Accessed online at: http://glcf.umd.edu/library/guide/aster_user_guide_v2.pdf.

Allen, M.R., Barros, V.R., Broome, J., Cramer, W., Christ, R., Church, J.A., Clarke, L., Dahe, Q., Dasgupta, P., Dubash, N.K., Edenhofer, O., Elgizouli, I., Field, C.B., Forster, P., Friedlingstein, P., Fuglestvedt, J., Gomez-Echeverri, L., Hallegatte, S., Hegerl, G., Howden, M., Jiang, K., Cisneros, B.J., Kattsov, V., Lee, H., Mach, K.J., Marotzke, J., Mastrandrea, M.D., Meyer, L., Minx, J., Mulugetta, Y., 'Brien, K.O., Oppenheimer, M., Pachauri, R.K., Pereira, J.J., Pichs-Madruga, R., Plattner, G.-K., Pörtner, H.-O., Power, S.B., Preston, B., Ravindranath, N.H., Reisinger, A., Riahi, K., Rusticucci, M., Scholes, R., Seyboth, K., Sokona, Y., Stavins, R., Stocker, T.F., Tschakert, P., van Vuuren, D., van Ypersele, J.-P., Blanco, G., Eby, M., Edmonds, J., Fleurbaey, M., Gerlagh, R., Kartha, S., Kunreuther, H., Rogelj, J., Schaeffer, M., Sedláček, J., Sims, R., Ürge-Vorsatz, D., Victor, D., Yohe, G., 2014. IPCC Fifth Assessment Synthesis Report - Climate Change 2014 Synthesis Report. 116.

Anderson, L.S., Anderson, R.S., 2016. Modeling debris-covered glaciers: response to steady debris deposition. The Cryosphere 10, 1105–1124.

Anderson, R.S., 2000. A model of ablation-dominated medial moraines and the generation of debris-mantled glacier snouts. Journal of Glaciology 46, 459–469. doi:10.3189/172756500781833025

Arendt, A., Bolch, T., Cogley, J.G., Gardner, A., Hagen, J.O., 2012. Randolph glacier inventory—a dataset of global glacier outlines: version 3.2. Global Land Ice Measurements from Space. Retrieved February 9, 2016. doi:10.1029/2012GL052712/full

Belò, M., Mayer, C., Smiraglia, C., Tamburini, A., 2008. The recent evolution of Liligo glacier, Karakoram, Pakistan, and its present quiescent phase. Annals of Glaciology 48, 171–176. doi:10.3189/172756408784700662

Benn, D.I., Bolch, T., Hands, K., Gulley, J., Luckman, A., Nicholson, L.I., Quincey, D., Thompson, S., Toumi, R., Wiseman, S., 2012. Response of debris-covered glaciers in the Mount Everest region to recent warming, and implications for outburst flood hazards. Earth Science Reviews 114, 156–174. doi:10.1016/j.earscirev.2012.03.008

Bolch, T., Buchroithner, M., Pieczonka, T., Kunert, A., 2008. Planimetric and volumetric glacier changes in the Khumbu Himal, Nepal, since 1962 using Corona, Landsat TM and ASTER data. Journal of Glaciology 54, 592–600. doi:10.3189/002214308786570782

Bolch, T., Kulkarni, A., Kääb, A., Huggel, C., Paul, F., Cogley, J.G., Frey, H., Kargel, J.S., Fujita, K., Scheel, M., Bajracharya, S., Stoffel, M., 2012. The State and Fate of Himalayan Glaciers. Science 336, 310–314. doi:10.1126/science.1215828

Bookhagen, B., Thiede, R.C., Strecker, M.R., 2005. Abnormal monsoon years and their control on erosion and sediment flux in the high, arid northwest Himalaya. Earth and Planetary Science Letters 231, 131-146.

Brock, B.W., Mihalcea, C., Kirkbride, M.P., Diolaiuti, G., Cutler, M.E.J., Smiraglia, C., 2010. Meteorology and surface energy fluxes in the 2005–2007 ablation seasons at the Miage debris-covered glacier, Mont Blanc Massif, Italian Alps. J. Geophys. Res. Atmos. 115, 112. doi:10.1029/2009JD013224

Collier, E., Nicholson, L.I., Brock, B.W., Maussion, F., Essery, R., Bush, A.B.G., 2014. Representing moisture fluxes and phase changes in glacier debris cover using a reservoir approach. The Cryosphere 8, 1429–1444. doi:10.5194/tc-8-1429-2014

Copland, L., Pope, S., Bishop, M.P., Shroder, J.F., Clendon, P., Bush, A., Kamp, U., Seong, Y.B., Owen, L.A., 2009. Glacier velocities across the central Karakoram. Annals of Glaciology 50, 41–49. doi:10.3189/172756409789624229

Deline, P., 2005. Change in surface debris cover on Mont Blanc massif glaciers after the “Little Ice Age” termination. Holocene 15, 302–309. doi:10.1191/0959683605hl809rr

Desio , A. An exceptional advance in the Karakoram-Ladakh region. Journal of Glaciology 2, 383–385.

Diolaiuti, G., Pecci, M., Smiraglia, C., 2003. Liligo Glacier, Karakoram, Pakistan: a reconstruction of the recent history of a surge-type glacier. Annals of Glaciology 36, 168–172. doi:10.3189/172756403781816103

Dunning, S.A., Rosser, N.J., McColl, S.T., Reznichenko, N.V., 2015. Rapid sequestration of rock avalanche deposits within glaciers. Nature communications 6, 7964.

Evatt, G.W., Abrahams, I.D., Heil, M., Mayer, C., Kingslake, J., Mitchell, S.L., Fowler, A.C., Clark, C.D., 2015. Glacial melt under a porous debris layer. Journal of Glaciology 61, 825–836. doi:10.3189/2015JoG14J235

Foster, L.A., Brock, B.W., Cutler, M.E.J., Diotri, F., 2012. A physically based method for estimating supraglacial debris thickness from thermal band remote-sensing data. Journal of Glaciology 58, 677–691. doi:10.3189/2012JoG11J194

Fushimi, H., Yoshida, M., Watanabe, O., Upadhyay, B.P., 1980. Distributions and Grain Sizes of Supraglacial Debris in the Khumbu Glacier, Khumbu Region, East Nepal. Journal of the Japanese Society of Snow and Ice 41, 18–25. doi:10.5331/seppyo.41.Special_18

Gao, B.-C., 1996. NDWI—A normalized difference water index for remote sensing of vegetation liquid water from space. Remote Sensing of Environment 58, 257–266. doi:10.1016/S0034-4257(96)00067-3

Gardelle, J., Berthier, E., Arnaud, Y., 2012. Slight mass gain of Karakoram glaciers in the early twenty-first century. Nature Geoscience 5, 322–325. doi:10.1038/ngeo1450

Gibson, M.J., Glasser, N.F., Quincey, D.J., Rowan, A.V., Irvine-Fynn, T.D., 2016. Changes in glacier surface cover on Baltoro Glacier, Karakoram, north Pakistan, 2001–2012. Journal of Maps 13, 100–108.

Hambrey, M.J., Bennett, M.R., Dowdeswell, J.A., Glasser, N.F., Huddart, D., 1999. Debris entrainment and transfer in polythermal valley glaciers. Journal of Glaciology 45, 69–86. doi:10.3198/1999JoG45-149-69-86

Hambrey, M.J., Quincey, D.J., Glasser, N.F., Reynolds, J.M., Richardson, S.J., Clemmens, S., 2008. Sedimentological, geomorphological and dynamic context of debris-mantled glaciers, Mount Everest (Sagarmatha) region, Nepal. Quaternary Science Reviews 27, 2361–2389. doi:10.1016/j.quascirev.2008.08.010

Heimsath, A.M., McGlynn, R., 2008. Quantifying periglacial erosion in the Nepal high Himalaya. Geomorphology 97, 5–23.

Immerzeel, W.W., van Beek, L.P.H., Bierkens, M.F.P., 2010. Climate Change Will Affect the Asian Water Towers. Science 328, 1382–1385. doi:10.1126/science.1183188

Kayastha, R.B., Takeuchi, Y., Nakawo, M., Ageta, Y., 2000. Practical prediction of ice melting beneath various thickness of debris cover on Khumbu Glacier, Nepal, using a positive degree-day factor. In Nakawo, M., Raymond, C., Fountain, A. (Eds.), Debris covered glaciers. IAHS Production, Wallingford.

Kirkbride, M.P., Deline, P., 2013. The formation of supraglacial debris covers by primary dispersal from transverse englacial debris bands. Earth Surf. Process. Landforms 38, 1779–1792. doi:10.1002/esp.3416

Kirkbride, M.P., Warren, C.R., 1999. Tasman Glacier, New Zealand: 20th-century thinning and predicted calving retreat. Global and Planetary Change 22, 11–28.

Leprince, S., Ayoub, F., Klingert, Y., Avouac, J.-P., 2007. Co-Registration of Optically Sensed Images and Correlation (COSI-Corr): an operational methodology for ground deformation measurements. IGARSS 1943–1946. doi:10.1109/IGARSS.2007.4423207

Lillesand, T., Keifer, R., Chipman, J., 2014. Remote Sensing and Image Interpretation. John Wiley and Sons, Chichester.

Mayer, C., Lambrecht, A., Belò, M., Smiraglia, C., Diolaiuti, G., 2006. Glaciological characteristics of the ablation zone of Baltoro glacier, Karakoram, Pakistan. Annals of Glaciology 43, 123–131. doi:10.3189/172756406781812087

McCarthy, M., Pritchard, H., Willis, I., King, G., 2017. Ground-penetrating radar measurements of debris thickness on Lirung Glacier, Nepal. *Journal of Glaciology* 1-13.

Meier, M.F. and Post, A., 1969. What are glacier surges? Canadian Journal of Earth Sciences 6, 807-817.

Mihalcea, C., Brock, B.W., Diolaiuti, G., D'Agata, C., Citterio, M., Kirkbride, M.P., Cutler, M.E.J., Smiraglia, C., 2008a. Using ASTER satellite and ground-based surface temperature measurements to derive supraglacial debris cover and thickness patterns on Miage Glacier (Mont Blanc Massif, Italy). Cold Regions Science and Technology 52, 341–354. doi:10.1016/j.coldregions.2007.03.004

Mihalcea, C., Mayer, C., Diolaiuti, G., D'Agata, C., Smiraglia, C., Lambrecht, A., Vuillermoz, E., Tartari, G., 2008b. Spatial distribution of debris thickness and melting from remote-sensing and meteorological data, at debris-covered Baltoro glacier, Karakoram, Pakistan. Annals of Glaciology 48, 49–57. doi:10.3189/172756408784700680

Mihalcea, C., Mayer, C., Diolaiuti, G., Lambrecht, A., Smiraglia, C., Tartari, G., 2006. Ice ablation and meteorological conditions on the debris-covered area of Baltoro glacier, Karakoram, Pakistan. Annals of Glaciology 43, 292–300. doi:10.3189/172756406781812104

Minora, U., Senese, A., Bocchiola, D., Soncini, A., D'Agata, C., Ambrosini, R., Mayer, C., Lambrecht, A., Vuillermoz, E., Smiraglia, C., Diolaiuti, G., 2015. A simple model to evaluate ice melt over the ablation area of glaciers in the Central Karakoram National Park, Pakistan.

Annals of Glaciology 56, 202–216. doi:10.3189/2015AoG70A206

Molnar, P., Anderson, R.S., Anderson, S.P., 2007. Tectonics, fracturing of rock, and erosion. J. Geophys. Res. Atmos. 112, F03014. doi:10.1029/2005JF000433

Nicholson, L., Benn, D.I., 2006. Calculating ice melt beneath a debris layer using meteorological data. Journal of Glaciology 52, 463–470. doi:10.3189/172756506781828584

Östrem, G., 1959. Ice melting under a thin layer of moraine, and the existence of ice cores in moraine ridges. Geografiska Annaler 41, 228–230. doi:10.2307/4626805

Pan, B.T., Geng, H.P., Hu, X.F., Sun, R.H. and Wang, C., 2010. The topographic controls on the decadal-scale erosion rates in Qilian Shan Mountains, NW China. *Earth and Planetary Science Letters*, *292*(1), pp.148-157.

Peizhen, Z., Molnar, P., Downs, W.R., 2001. Increased sedimentation rates and grain sizes 2|[ndash]|4|[thinsp]|Myr ago due to the influence of climate change on erosion rates. Nature 410, 891–897. doi:10.1038/35073504

Quincey, D.J., Copland, L., Mayer, C., Bishop, M., Luckman, A., Belò, M., 2009. Ice velocity and climate variations for Baltoro Glacier, Pakistan. Journal of Glaciology 55, 1061–1071. doi:10.3189/002214309790794913

Ranzi, R., Grossi, G., Lacovelli, L., Taschner, S., 2004. Use of multispectral ASTER images for mapping debris-covered glaciers within the GLIMS project. In *Geoscience and Remote Sensing Symposium, 2004, IGARSS 2004 Proceedings. 2004 IEEE International* 2, 1144-1147.

Reid, T.D., Brock, B.W., 2010. An energy-balance model for debris-covered glaciers including heat conduction through the debris layer. Journal of Glaciology 56, 903–916. doi:10.3189/002214310794457218

Rounce, D.R., McKinney, D.C., 2014. Debris thickness of glaciers in the Everest area (Nepal Himalaya) derived from satellite imagery using a nonlinear energy balance model. The Cryosphere 8, 1317–1329. doi:10.5194/tc-8-1317-2014

Rowan, A.V., Egholm, D.L., Quincey, D.J., Glasser, N.F., 2015. Modelling the feedbacks between mass balance, ice flow and debris transport to predict the response to climate change of debris-covered glaciers in the Himalaya. Earth and Planetary Science Letters 430, 427–438. doi:10.1016/j.epsl.2015.09.004

Scherler, D., Bookhagen, B., Strecker, M.R., 2011. Spatially variable response of

Himalayan glaciers to climate change affected by debris cover. Nature Geoscience 4, 156–159. doi:10.1038/ngeo1068

Scherler, D., 2014. Climatic limits to headwall retreat in the Khumbu Himalaya, eastern Nepal. Geology 42, 1019–1022.

Searle, M.P., Parrish, R.R., Thow, A.V., Noble, S.R., Phillips, R.J., Waters, D.J., 2010. Anatomy, age and evolution of a collisional mountain belt: the Baltoro granite batholith and Karakoram Metamorphic Complex, Pakistani Karakoram. Journal of the Geological Society 167, 183–202. doi:10.1144/0016-76492009-043

Seong, Y.B., Owen, L.A., Caffee, M.W., Kamp, U., Bishop, M.P., Bush, A., Copland, L., Shroder, J.F., 2009. Rates of basin-wide rockwall retreat in the K2 region of the Central Karakoram defined by terrestrial cosmogenic nuclide 10 Be. Geomorphology 107, 254-262.

Shea, J.M., Immerzeel, W.W., Wagnon, P., Vincent, C., Bajracharya, S., 2015. Modelling glacier change in the Everest region, Nepal Himalaya. The Cryosphere 9, 1105–1128. doi:10.5194/tc-9-1105-2015

Shekhar, M.S., Chand, H., Kumar, S., 2010. Climate-change studies in the western Himalaya. Annals of Glaciology 51, 105–112. doi:10.3189/172756410791386508

Shroder, J.F., Bishop, M.P., Copland, L., Sloan, V.F., 2000. Debris-covered Glaciers and Rock Glaciers in the Nanga Parbat Himalaya, Pakistan. Geografiska Annaler: Series A, Physical Geography 82, 17–31. doi:10.1111/j.0435-3676.2000.00108.x

Soncini, A., Bocchiola, D., Confortola, G., Minora, U., Vuillermoz, E., Salerno, F., Viviano, G., Shrestha, D., Senese, A., Smiraglia, C., Diolaiuti, G., 2016. Future hydrological regimes and glacier cover in the Everest region: The case study of the upper Dudh Koshi basin. Science of The Total Environment 565, 1084–1101 doi:10.1016/j.scitotenv.2016.05.138

Tovar, D.S., Shulmeister, J., Davies, T.R., 2008. Evidence for a landslide origin of New Zealand's Waiho Loop moraine. Nature Geoscience 1, 524–526. doi:10.1038/ngeo249

Watson, C.S., Quincey, D.J., Carrivick, J.L., Smith, M.W., 2016. The dynamics of supraglacial ponds in the Everest region, central Himalaya. Global and Planetary Change 142, 14–27. doi:10.1016/j.gloplacha.2016.04.008

Winkler, S., Matthews, J.A., 2010. Observations on terminal moraine-ridge formation during recent advances of southern Norwegian glaciers. Geomorphology 116, 87–106.

Zhang, Y., Fujita, K., Liu, S., Liu, Q., Nuimura, T., 2011. Distribution of debris thickness and its effect on ice melt at Hailuogou glacier, southeastern Tibetan Plateau, using in situ surveys and ASTER imagery. Journal of Glaciology 57, 1147–1157. doi:10.3189/002214311798843331